AIAA SciTech Forum
7-11 January 2019, San Diego, California
AIAA Scitech 2019 Forum

10.2514/6.2019-2284

Artificial Light Detection as a Method for Poacher Detection from an Unmanned Aerial Vehicle

Alex Bernard,* Gabi Sciuchetti,* Christopher Lynch,* Ang Sherpa†
University of Washington, Seattle, WA, 98195, USA

Joel Reiter,‡
Vulcan Inc., Seattle, WA, 98104, USA

Christopher W. Lum§
Autonomous Flight Systems Laboratory, University of Washington, Seattle, WA, 98195, USA

Atypical methods of detection are required to accurately and consistently detect poachers in the African Savannah. A promising idea is utilizing unmanned aerial systems (UAS) to detect and monitor these poachers. This paper investigates the design and development a sensor system that can be mounted on a fixed wing UAS and integrated with other optical sensors. A trade study was conducted that determined that a light detection sensor had a strong possibility of success, but had to be developed using a light sensitive camera and a filtration script. Signal to noise ratio (SNR) was determined to be the main quantifiable metric for determining success, and initial feasibility calculations indicated that the intended design would perform well. The system was then successfully prototyped for flight testing. Several variables were measured including type of light source, weather conditions, camera mount angle, and direct or indirect light. Flight tests were successfully conducted, and post processing scripts were developed to flag images with light and determine SNR. It was found that the system delivered a higher SNR under cloudy weather, gave a decreasing SNR but increasing probability of detection by increasing mount angle and produced a higher SNR with light sources shined at the ground as opposed to directly at the UAS. Flight testing also determined the optimal exposure value of the system.

*Undergraduate, Department of Aeronautics and Astronautics, Seattle, WA 98195, AIAA Student Member.
†Undergraduate, Department of Electrical Engineering, Seattle, WA 98195
‡Lead Electrical Engineer, Vulcan Inc., Seattle, WA, 98104
§Research Assistant Professor, Department of Aeronautics and Astronautics, Seattle, WA 98195, Member AIAA.

Nomenclature

A	Area (m^2)	$beam$	Flashlight Beam
Ab	Absolute Sensitivity Threshold	$disp$	Dispersed
c	Speed of Light (m/s^2)	ext	External to Camera/Lens body
d	Distance or Length (m)	$emit$	Emitted
D	Temporal Dark Noise (e^-)	int	Internal to Camera/Lens body
EV	Exposure Value	$flash$	Flashlight Body
h	Planck's Constant (m^2kg/s)	f, l	Light Emitting Part of Flashlight
L	Luminosity (W)	gc	Ground Captured by Lens
n	Number of Pixels	gr	Ground Recorded by Sensor
N_r	Electrical Noise (e^-)	$light$	Light Output from Flashlight
P	Number of Photons	l	Length
QE	Quantum Efficiency	$lens$	Camera Lens
r	Radius (m)	$moon$	Moon
t	Shutter Speed (s)	ref	Reference
α	albedo	sky	A Moonless, Starlit Sky
η	Luminous efficacy (lumen/W)	$sens$	Camera Sensor
λ	Wavelength (Hz)	$shutter$	In the Duration of the Shutter Speed
θ	Angle (rad)	UAS	Unmanned Aerial System, with Camera Onboard
Φ_v	Luminous Flux (lumen)	w	Width

I. Introduction

A. Problem Definition

Poaching is a pressing issue in the world today. Poachers break laws and kill endangered animals, pushing them ever-closer to extinction and reducing the Earth's biodiversity, something that harms all of Earth's inhabitants. Elephants, for example, are a keystone species which means they impact dozens of other species and the general environment around them, including humans. By continuing to allow poaching, keystone species like elephants are becoming extinct which is doing irreversible damage to the Earth. Additionally, profits from poaching are sometimes used to fund terrorist groups, a direct way poaching is causing harm to humans.[1]

The black rhino population has been reduced by 97.6 percent since 1960, largely due to poaching. Annually, 30,000 to 38,000 elephants are killed for their ivory. At current poaching rates, iconic African wildlife like elephants and rhinos could be extinct within twenty years.[2] The tactics poachers use are often sadistic in nature. For example, elephants will gather around an elephant that has died or is dying in a sort of death ritual. Poachers take advantage of this and will kill or wound an elephant, wait for others to gather around in sadness, and then kill more elephants.[1] Animals in all shapes and sizes, from bears to manta rays, are killed or abused by poachers to have parts of them sold for use in traditional medicines, meals, charms and as decorations. There is no need to continue this senseless slaughter, and humans should have a responsibility to stop it.

Poaching can happen as close as your backyard, or as far away as Siberia. However, Africa is a specific area of concern due to large populations of vulnerable animals as well as huge areas that are difficult to police. A sensible solution is the use of unmanned aerial systems (UAS) to survey large swaths of land. These UAS systems typically carry an optical system (camera) and a machine learning algorithm to identify poachers, and then report back to a base where park rangers or appropriate authorities can be alerted. This poses many challenges in accurate identification, power requirements to sustain on board computing, and the limitation of working during daylight hours.

B. Literature Review

There are various groups working on implementation of a UAS for anti-poaching operations. One of the earlier groups to begin this research used visual and thermal cameras on a UAS to monitor areas for rhinoceros poaching activity. Their conclusion was that a UAS is effective "as a tool for surveillance of sensitive areas, for supporting field anti-poaching operations, as a deterrent tool for poachers and as a complementary method for rhinoceros ecology research."[3] Air Shepard is another project whose purpose is to utilize UAS to combat poaching. They operate in three separate countries is Southern Africa and utilize high resolution and infrared cameras to detect poachers.[4] Another effort that is currently utilizing UAS for anti-poaching operations is a project that is funded by a $5 million grant from Google and the World Wildlife Fund. Micro Aviation SA has produced a UAS called the BatHawk that is being operated for poacher patrolling in national parks in several different countries. The UAS is operated by the company UAV & Drone Solutions and it relies on thermal imagery for poacher detection. It has been moderately successful in finding and deterring poachers in the protected areas where it is used. This effort has also indentified several problems with poacher detection from a UAS relating to the probability of detection as well as other practical issues.[5]

Many groups have investigated the usage of UAS for similar missions such as search[6] and rescue,[7] persistent surveillance,[8] wildfire detection,[9] precision agriculture,[10] and aerial mapping.[11] For this project, one of the practical issues is how best to deploy the UAS for anti-poaching operations. This concern has prompted analyst groups such as Wildeas to study how best to integrate technological solutions into stopping poaching.[12] Another solution to practical issues is to develop machine learning algorithms to enable more reliable detection of poachers during long flights. Work has been done by researchers at the University of Southern California to develop machine learning algorithms which will be utilized by Air Shepard to fight poaching.[13] These researchers are showing that machine learning can be a valuable tool that is ready to be deployed even in areas with complex terrain.[14] Their analysis of 180,000 individual poachers and animals in 40,000 images provides a deployable tool to be used for traditional visual sensing methods, however there is still room to improve detection probability through the use of additional, less traditional sensing techniques.[13]

Vulcan, Inc. aims to integrate a non-traditional imaging sensor on board a UAS to be used for anti-poaching operations under conditions where it can function outside the norm and increase the probability of detection while taking advantage of machine learning tools and avoiding other practical issues. With such a broad problem there are virtually endless ways of approaching possible solutions. This is why an initial trade study of various non-optical sensors was completed, considering magnetometers, radar systems, cell phone detection, artificial light detection, and gunshot detection. Due to cost and precision considerations, the decision was made to move forward with artificial light detection.

Traditional light detection methods make use of photodioides that return either 'on' or 'off'. However, to be able to pinpoint the location of the light source, as well as to detect light as dim as that which is expected to be seen from above, a more sensitive method is necessary. Little work has been done to attempt to use a low light imaging camera together with a processing algorithm solely to isolate and detect sources of light. This project hopes to change that.

C. Aerospace Context

In the modern aerospace industry, UAS are becoming more and more important as a tool for a variety of customers. A UAS can fulfill many versatile roles. They have applications ranging from military roles to entertainment for hobbyists, and everything in-between. The demand for new development will only increase in the future: "The [UAS] market is expected to grow US $ 51.85 billion by 2025 from US $ 11.45 billion in 2016."[15] It is therefore vital that aerospace engineers and their employers are able to anticipate future needs and prepare to develop solutions that fit customer demands. A UAS for nearly any application will need on board sensor equipment to ensure it can fulfill its role. Additionally, any UAS that engineers develop will need to undergo flight testing so any potential issues can be resolved and the UAS can be delivered to customers with optimal performance.

D. Functional Requirements/Customer Specifications

The artificial light detection payload was designed to fulfill certain specifications set by Vulcan, Inc. Of key concern were mass, power usage and cost. The maximum allowable mass was set to be below 1 kg. The power usage should be sufficiently low as to not dramatically reduce the endurance of the final aircraft below

5 hours. This both of these factors would allow the aircraft to stay aloft for sufficient time to efficiently patrol large areas during its final use. Our budget was fixed at $4000 and could not be exceeded, so the sensor payload needed needed to cost less than this to leave budget for other project expenses. In terms of deliverables, Vulcan, Inc. wished to have a working prototype with sets of data from flight testing that could be used to train machine learning algorithms for target detection.

E. Design Approach

With such a broad problem to tackle, the design approach required thought and planning in order to finish the project on time. The first step in the process was to conduct a broad survey of the problem, learning about the *modus operandi* of poachers to better understand ways of detecting them, as well as looking into other past work and various sensing technologies. After this broad survey, several candidate sensing technologies were identified and a trade study was conducted weighing the various options against each other. After light detection was selected, team members conducted an in-depth feasibility study, including some initial testing to verify the validity of artificial light detection as a strategy for poacher detection. Once the in-depth feasibility analysis was complete, work began on both the physical integration of the payload as well as its software infrastructure, while simultaneously conducting ground tests. These ground tests provided direction for the final phase of the project, which was flight testing. These flight tests were completed in order to further prove validity and provide Vulcan with the image database that they requested.

According to our research, there were had been no other investigations into artificial detection from a UAS similar to our application. Thus, this was a novel project that required thought and testing in order to ensure success. Ultimately, the success of this payload will be measured in poachers stopped and animals saved, however as a testing metric its success will be measured on Signal-to-Noise Ratio (SNR) and the ability for a human to clearly see a source of artificial light in the data outputs.

II. Design

A. Sensor Trade Study

A survey of sensors that may be suited to the application was completed, and several of those sensors were selected for further in depth inquiry. The sensors chosen are listen in Fig. 1, along with comments and numerical scores of various components. The numerical scores were obtained by comparing the values for each sensor to known constraints to decide which would be best and worst, and fixing those at the two ends of the spectrum, and then interpolating to find scores for all values between the extremes. Once scores for individual components were found, these were combined into an overall feasibility score.

The total feasibility score for each sensor was found by weighting each component individually as shown in Table 1. The percentage weight of each component was determined through a combination of customer specifications and design requirements. The most important components to a sensor's potential is the sensitivity (range in which sensor is expected to perform accurately), precision (fidelity with which the sensor can detect when under ideal operating conditions), and susceptibility to noise. For example, a magnetometer can detect magnetic materials from very far away, but has a hard time distinguishing the magnetic signature of a car versus magnetic minerals in the Earth below the car. Occurrence likelihood describes how probable the case in which detection can be successful occurs. For example, gunshot detection can be incredibly accurate, but is only successful if the UAS is within range of detection when the gunshot occurs. Comparatively, LiDAR will always be able to detect people or vehicles when it is within range. Occurrence likelihood is the only variable rated on a scale of one to three as opposed to one to ten, as there was little distinction between what would yield a score of five or six.

Variables		Gunshot Detection: AVS	Velodyne LiDar Puck	Echodyne MESA-DAA	Magnetometer	Millimeter Wave	Cell Phone Detection	Artificial Light Detection
Primary Function(s) of Sensor		Detects gunshots (potentially other sounds as well) and the general area they originated	Uses laser point mapping to find anomolies (i.e. straight lines)	Long-range radar used to detect moving objects. Designed to detect moving objects in air.	Changes in magnetic field helps detects metallic object. Unfortunately Gem's sensor average AGL is 60m.	Uses frequency between 30Ghz and 300Ghz to detect of object. Similar to Echodyne.	Short range device to monitor cell signal	Use high contrast high gain images to detect light
Mass	Comments	150g	830 g	730 g	890g	<500gram	<500g	400 g
	Score	10	5	6	5	7	7	8
Price	Comments	60000 USD	8,000 USD	10,000 USD	4000 USD	$300	$250	900
	Score	1	3	2	6	10	10	9
Precision	Comments	+/- 20 m	+/- 3 cm	+/- 3.25 m	+/- 15 m	+/- 2m	<= .05 mw	+/- 0.3 cm
	Score	4	10	7	5	7	9	10
Noise Susceptibility	Comments	low-mid	low	medium/high	high	high	low	low/mid
	Score	9	10	5	1	5	7	7
Power Usage	Comments	1-1.5W	8 watts	35 watts	14 W	12.5 W	9V battery	20 W
	Score	10	9	4	7	8	10	7
Sensitivity	Comments	2km, 500m for best detection	Range up to 100m	Range up to 3.4 km	50 m	depends on magnetic noise	130 ft (40m)	100-120m (potentially)
	Score	9	4	10	3	5	2	5
Ease of Integration	Comments	Easy - medium	Easy	medium, 'plug and play'	easy - medium	medium-difficult	high	easy
	Score	9	10	9	6	8	2	8
Durbility	Comments	~IP67	IP67	IP68	N/A	IP69K	N/A	IP61
	Score	7	8	9	5	10	5	6
Occurance Likelyhood	Comments	only during gunshot	if anything is there, will see	If in view it will see	Only if using vehicle	difficult to classify object	If within range should detect	only if carrying flashlights
	Score	1	3	3	2	1	2	2
Processing Power	Comments	very low (peak)	complex mapping	complex mapping	fairly low (peak in noise)	medium	very low	very low (peak)
	Score	10	1	2	8	6	10	10
Total Score		744	670	619	447	649	629	717

Fig. 1: A trade study of the most viable sensor options.

Table 1: Comparative weighting of trade study components to characterize final score.

Mass	10%
Price	5%
Precision	14%
Noise Susceptibility	14%
Power Usage	10%
Sensitivity	16%
Ease of Integration	7%
Durability	9%
Occurrence Likelihood	7%
Processing Power	8%

As shown in Fig. 1, the AVS Gunshot Detection has the highest total score. It was capable of detecting gunshots or other loud sounds and determine the location of their origin with surprising accuracy. It appeared to be a highly sensitive sensor with accurate enough precision to return the necessary results. However, the price was prohibitive for the project, and so it was pulled out of the running. In the future it may be possible to pursue development of a gunshot detection or sound event recognition system given a longer timescale and larger budget. The Velodyne LiDAR Puck was also a strong contender, with high occurrence likelihood

and precision, but a low sensitivity and high weight ultimately put it out of the running. The Echodyne MESA-DAA had a very high range that piqued the interest of the project sponsors, however the time to acquire the sensor was well outside of the project timescale. Thus, unfortunately this sensor could not be pursued for this project. Magnetometers were deemed to be too inaccurate due to background noise. There was also additional difficulty with magnetometers because of interference of the UAS motor, which can be remedied by towing the magnetometer below the UAS. This style of operations is outside of the realm of possibility for the planned flight vehicles and operating parameters, decisively putting magnetometers out of the running. Millimeter wave sensors were found to be lacking in sensitivity, as with cell phone detection. Artificial light detection presented some difficulty in that there were no sensors designed to detect light at far distances. Instead of attempting to find an off the shelf sensor, the fabrication of a light detection sensor was investigated. Evaluating light detection using a high contrast CMOS camera with data processing algorithms yield a high precision sensor with low data processing requirements and a relatively low price. Based on the completed trade study, artificial light detection was chosen as the sensor to move forward with.

B. Feasibility Analysis

The area covered by a flashlight shone at the ground can be approximated as an ellipse, as shown in Fig. 2. The distance to edges of the ellipse from the flashlight can be represented as $h_{light} * tan(\theta_{flash} \pm \theta_{beam})$, and the center as $h_{light} * tan(\theta_{flash})$. The width can then be represented as $d_{center} * tan(\theta_{beam})$.

$$A_{light} = \pi r_1 r_2 = \pi(d_{center} tan(\theta_{beam}))(h_{light} tan(\theta_{flash} + \theta_{beam}) - h_{light} tan(\theta_{flash})) \quad (1)$$

Using Eqn. 1, the area of the illuminated ground can be found in terms of the angle of the flashlight relative to the ground, the height of the flashlight above the ground, and the beam width of the flashlight.

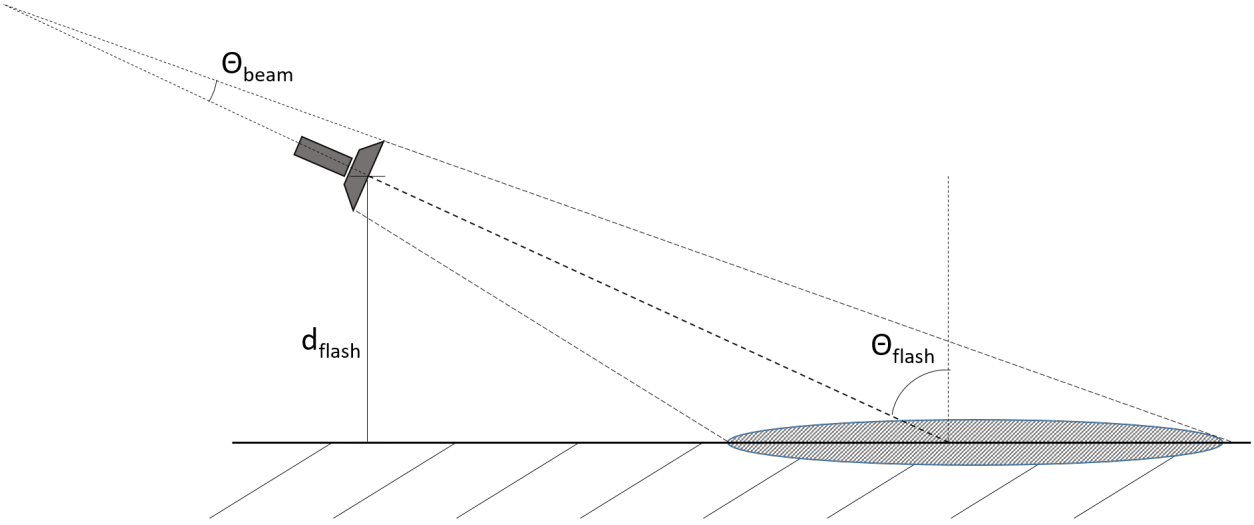

Fig. 2: Diagram of flashlight directed at ground and reflected area.

The camera lens focuses photons from the external lens to the internal lens. Once past the internal lens, the photons bounce off of the camera sensor and register as electrical impulses. Since the camera sensor is rectangular, but the lens is circular, not all of the data collected from the lens will be used. Additionally, if the sensor used is not a full sensor (1"), but a crop sensor, less of the captured data will be recorded. Figure 3 shows the path of light as it enters the camera. The ratio of data used from the internal lens is simply an area ratio of $A_{sensor}/A_{int,lens}$. The area of the sensor is defined as in the numerator of Eqn. 2, where d_{pixel} is the length of a pixel edge, and n_{total} is the total number of pixels in the image.

$$\frac{A_{int,used}}{A_{int}} = \frac{d_{pixel}^2 n_{total}}{\pi r_{int}^2} \quad (2)$$

The ratio of the useful area on the external lens can then be found by assuming that lens area is proportional to the ratio of useful area.

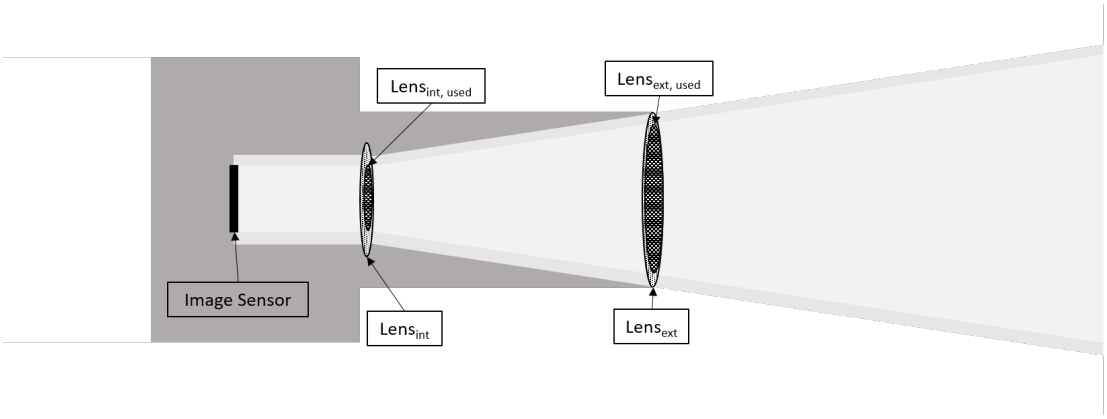

Fig. 3: A diagram of internal and external camera lenses.

$$\frac{A_{ext,used}}{A_{ext}} = \frac{A_{int,used}}{A_{int}} \frac{A_{ext}}{A_{int}} = \frac{d_{pixel}^2 n_{total} (\pi r_{ext}^2)^2}{(\pi r_{int}^2)^2} \tag{3}$$

The total ground area captured by the lens can be calculated as a circle with a radius of the height of the camera multiplied by the tangent of the field of view of the lens. The ground area recorded by the sensor can then be calculated by using area captured by the lens and the ratio of useful area on the external lens, as shown in Eqn. 4.

$$A_{gr} = \frac{A_{ext,used}}{A_{ext}} A_{gc} = \frac{A_{ext,used}}{A_{ext}} \pi (d_{lens} tan(\theta_{lens}))^2 \tag{4}$$

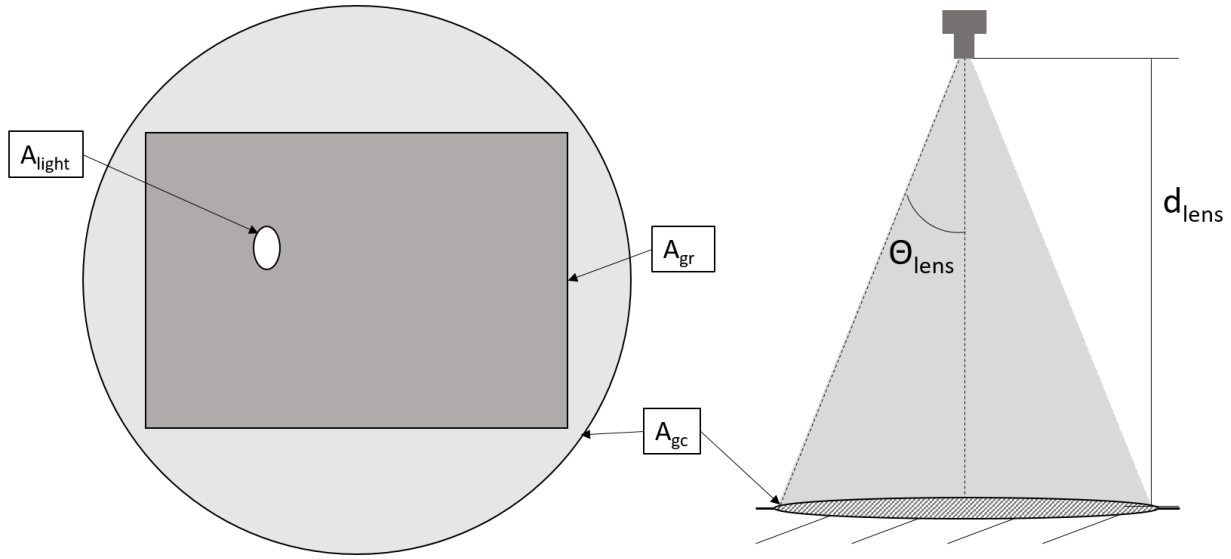

Fig. 4: Ground area captured by sensor, shown from above (left) and the side (right)

The number of illuminated pixels (assuming a consistently bright illuminated area) can be calculated by finding the ratio of illuminated area to total ground area captured by the sensor, and multiplying this by the total number of pixels, as shown in Eqn. 5.

$$n_{light} = \frac{A_{light}}{A_{gr}} n_{total} \tag{5}$$

Luminous flux is a measure of the total amount of visible light emitted from a source, while luminous efficacy is a measure of how efficiently a source produces light. The power of a light source, or luminosity,

is defined as the luminous flux per luminous efficacy. The photons emitted per second from a light source is defined as shown in Eqn. 6.

$$P_{emit} = \frac{L * \lambda}{h * c} = \frac{\Phi_v \lambda}{\eta h c} \tag{6}$$

The light reflected from the ground is simply the product of the albedo of the ground and the total photons emitted. Assuming the photons disperse radially from a uniform reflected light source, the photons per second per meters^2 drop off with distance squared as shown in Eqn. 7.

$$P_{disp} = \frac{P_{ref}}{d_{lens}^2} = \frac{P_{emit} * \alpha}{d_{lens}^2} \tag{7}$$

The photons incident on the relevant area of the lens can then be found by multiplying the useful area of the external lens by the dispersed photons. Of these incident photons, the camera can only detect some finite amount. The fraction of photons detected is defined as the quantum efficiency; multiplying the quantum effiency by the shutter speed and the incident photons per second yields the photons detected during a singular shutter, seen in Eqn. 8.

$$P_{shutter} = P_{disp} * A_{ext,used} * QE * t \tag{8}$$

Assuming that the photons incident on the sensor are concentrated in pixels corresponding to the illuminated pixels, the photons detected per illuminated pixel can be found by dividing the pixels detected from the light source by the number of illuminated pixels.

Similar to the light source, the power of the ambient light can be calculated using the luminosity of a full moon and a moonless sky and the luminous efficacy of the sky. Using Eqn. 6 and multiplying by the albdedo as discussed for the flashlight, the photons detected per pixel due to ambient light can be calculated. Because ambient illumination is assumed to be constant across the ground, no significant photon dispersion is expected.

The camera sensor will not only experience noise due to ambient light, but also due to dark current and electrical noise. Dark current refers to variations that occur in pixel brightness when the picture has no light sources (e.g. a picture taken with the lens cap on). Electrical noise is due to circuitry in the camera or sensor that causes random variation in pixel brightness.

The signal to noise ratio (SNR) represents the strength of the detected light of the flashlight compared to the noise in the photo, and can be used to predict likelihood of successful detection. The SNR is defined in Eqn. 9. The electrical noise can be computed using the absolute sensitivity threshold of a camera (at which the SNR is equal to 1), and solving for N_r.

$$SNR = \frac{P_{shutter}}{(P_{disp} A_{ext,used} + \alpha(P_{moon} + P_{sky})) * QE * t + Dt + N_r^2} \tag{9}$$

While signal to noise ratio gives a good indicator of whether detection will be possible, the relative size of the signal to the noise also governs detection probability. Imperfections in sensors cause 'hot pixels', which are single pixels that appear white regardless of camera input. If the signal took up only one pixel in the image, it would appear indistinguishable from these 'hot pixels', which would significantly affect the probability of detection. Figure 5 shows the predicted drop off of pixels as the UAS altitude is increased, along with a 0.05% threshold, above which the signal is deemed to be easily detectable. The signal size decreases below this threshold at approximately 375 m, at which point it may be detectable, but detection probability starts to drop off as altitude increases from there. However, 375 m is far above anticipated operating parameters, so signal size is unlikely to be a parameter that impacts detection probability.

C. Aperture and Shutter Speed Selection

Camera setting selection governs the amount of light that the camera sensor is exposed to, which correlates to how bright an image appears. The amount of light that is incident on the camera sensor is referred to as the image exposure. Exposure value (EV) is a scalar that represents the combination of camera parameters, such that all combinations that result in the same exposure have the same EV. Two camera parameters are generally considered when computing EV: aperture and shutter speed.

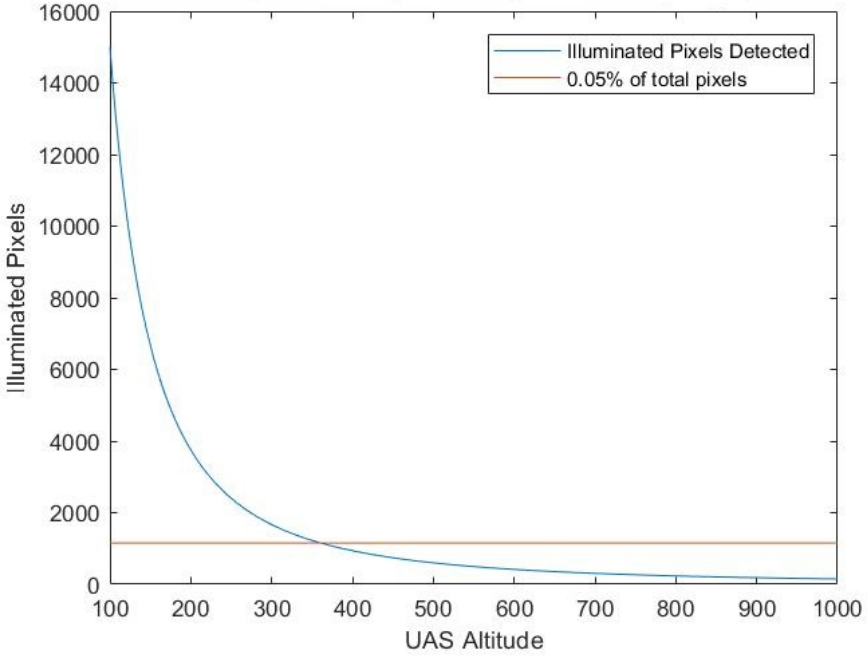

Fig. 5: Predicted drop off of signal size with increased altitude.

Changing the aperture of the camera changes how wide the internal camera shutter opens. By using a 'wide' aperture, which corresponds to a low f-stop number (i.e. f/1.4 or f/2.8), the shutter has a wide opening and so lets in a lot of light, making the overall image brighter. Comparatively, 'narrow' apertures, corresponding to a high f-stop (i.e. f/16 or f/22), will let in less light. Aperture also governs the depth of field of an image, which refers to how deep the area that appears in focus is. A very narrow aperture will have a large depth of field, where the entire image will appear in focus, and a wide aperture will have a shallow depth of field, where the background and of the image will be blurred.

The shutter speed used to take an image describes how long the shutter remains open for. The longer the shutter speed is, the more light it lets in, and the brighter the resultant image will be. A long shutter speed lends itself more to taking images of stationary objects while stationary, while a short shutter speed is better for taking images of fast moving objects or while the camera is moving quickly. Using a long shutter speed to take an image of a fast moving object will result in considerable blur around the object.

Two pictures with the same EV can still look drastically different; as aperture and shutter speed each individually change image characteristics that are not related to the image exposure. For example, and image taken at f/1.4 and 1/1000 seconds will have a narrow depth of field, but any motion that is in the field of focus will be sharp, while an image taken at f/11 and 1/15 seconds has the same exposure value, so will be equally bright, but will have a wide depth of field, with any motion blurred.

In order to increase the signal to noise ratio as much as possible, any light source (signal) should be as exposed as possible, while the background noise should be as dark as possible. However, the camera sensor is not capable of measuring an infinite amount of light, the brightest a given pixel can be is pure white, which represents a physical limit on the sensing capability of the camera; this cap is referred to as the saturation limit. Two simulated images with varying EVs are shown in Figure 6. In both images, the signal has reached the saturation limit, but the signal to noise ratio is much higher for the higher EV image. Increasing the EV once the signal is fully saturated cannot increase the recorded magnitude of the signal, so only increases the amount of noise in the image.

The EV must thus be carefully balanced to keep the signal fully saturated while keeping the noise as low as possible. With an exposure value chosen, aperture and shutter speed can be deduced by tolerance for blur and depth of field requirements.

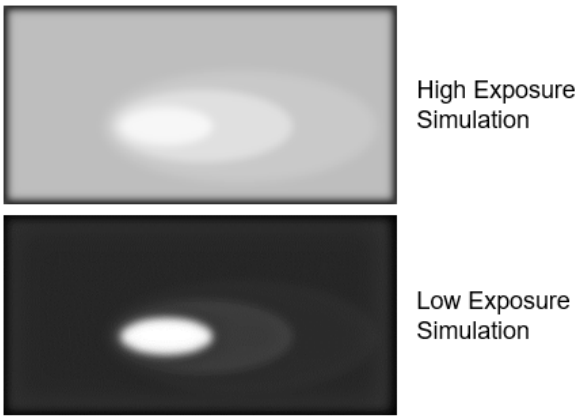

Fig. 6: A simulation of high and low exposure images.

III. Prototype

A. System Architecture

1. Overall System Architecture

A signal flow diagram between electronic components is displayed in Figure 7. The components in the UAV are comprised of a Blackfly GigE monochrome camera, a Raspberry Pi 3, a strobe light, red, green, and white LED lights, LiPo batteries, a portable powerbank, and a circuit built to connect all devices (excluding the Raspberry Pi) to a single battery. The maximum amperage of $2.5A$ supplied to the Raspberry Pi was not sustainable by the circuit wire due to the internal resistance of the wire, therefore, a power-bank with a constant output of $12V$, $2.5A$ was used to power the Raspberry Pi. All the electrical components used in the system were bought off the shelf. A C++ script was run on the Raspberry Pi to capture images and save them onto a 64Gb USB, which was removed after flight. The photos on the USB where then filtered using a Matlab script designed to detect light sources in images.

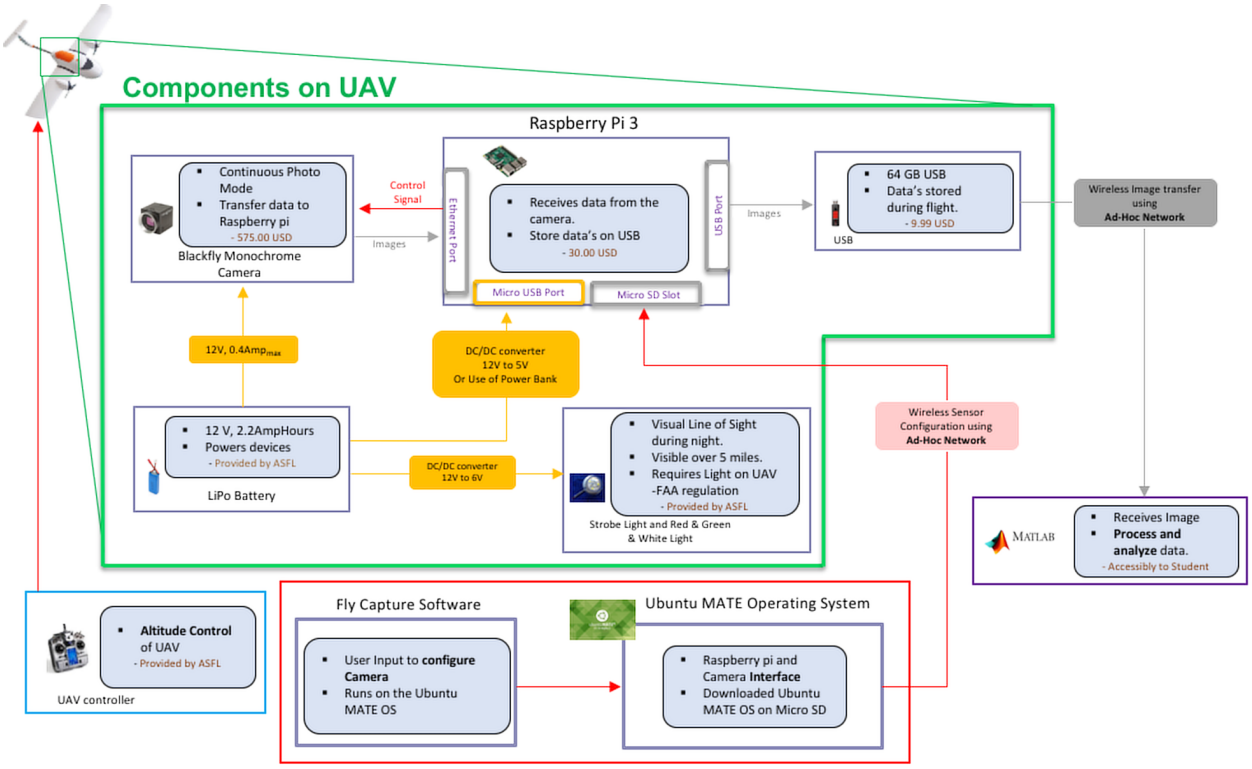

Fig. 7: A signal flow chart of the entire system.

2. *Electronics*

As each flight test requires a maximum of 12 minutes, a suitable LiPo Battery was chosen to last for more than an hour. As shown in Figure 9, a OKR - T/3 Series Buck Converter was chosen to step down to the required $6V$ to power the strobe light and the red, green, and white LEDs. Since the Raspberry Pi was powered by the power-bank, the load on the buck converter, with an output capacity of $15W$, was reduced. The Buck converter features an input voltage range of 4.5 to 14 V_{DC}, programmable output voltage from 0.591 to 6.0 V_{DC}, and a conversion efficiency of 93%. The control pin was left open to enable the buck converter. With the high efficiency of the Buck Converter, less power was consumed causing less heat to be released compared to the linear regulator. The OKR - T/3 Series are not internally fused. Therefore, to avoid injury to personnel or any expensive equipment, external fast-blow fuses were attached in-line with the components.

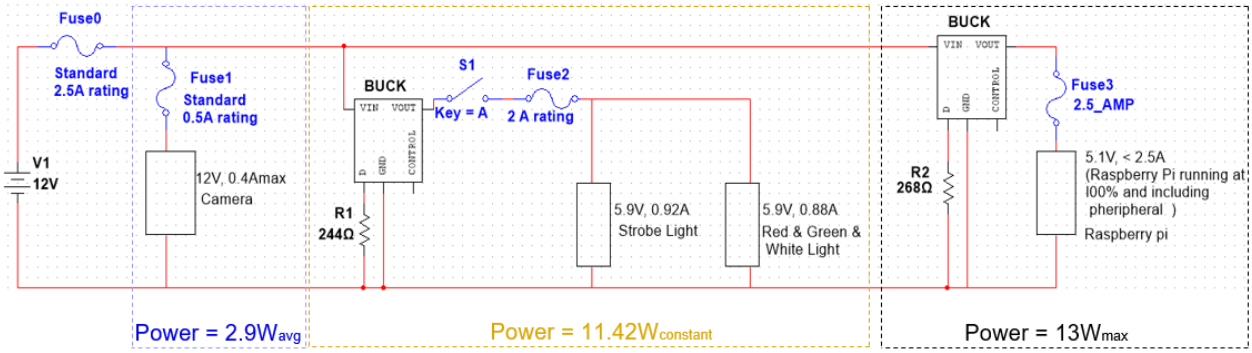

Fig. 8: A complete schematic design of the circuit.

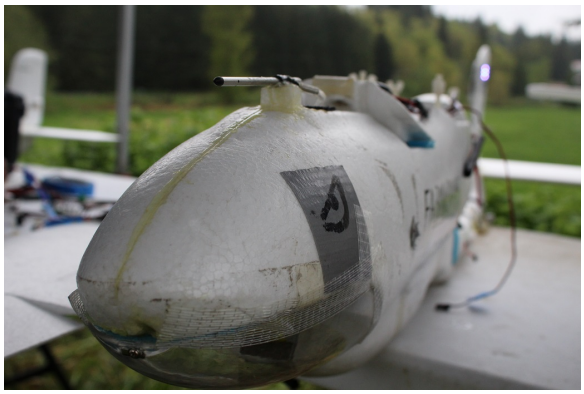

(a) The aircraft with the camera mounted in the nose behind a clear nose cone.

(b) A team member working on the interior connections for the payload.

Fig. 9: Images of the aircraft and integrated payload during flight test operations.

3. Aircraft

In order to complete the necessary flight testing, the team acquired a fixed wing UAS from the University of Washington Autonomous Flight Systems Laboratory (AFSL) and began the process of integrating the payload for testing. The model of UAS was a Finwing Sabre, and the camera was integrated into the nose where it was covered by a clear nose cone. In the nose cone it was possible to set the camera on several different fixed mounts to test different mount angles in a fixed, forward facing view. Flight testing was planned to occur mostly at night, so in order to comply with FAA regulations and to comply with FAA night waiver stipulations (which will be discussed in a later section) the aircraft was equipped with standard navigation lights. A strobe light was installed on the aft part of the aircraft, with standard solid red, green and white lights on the wing tips and tail of the aircraft, positioned such that they were visible from all angles. The lights were also visible for the minimum 3 statute miles as required by the FAA.

Fig. 10: The UAV with lights.

4. GCS Components

The aircraft was operated directly via a pilot on the ground for take-off, and once in the air, control was transferred to a ground control station which used the Ardu-Pilot Mission Planner software to control the aircraft. The aircraft followed a series of pre-programmed waypoint to fly around a field at the test site that allowed the camera to image test articles which had been set up throughout the field. In the sample waypoint file below, test articles would have been set up at points 4, 8 and 12, and would have come into view of the camera at different times during the approach to those points, depending on what angle the camera was mounted at.

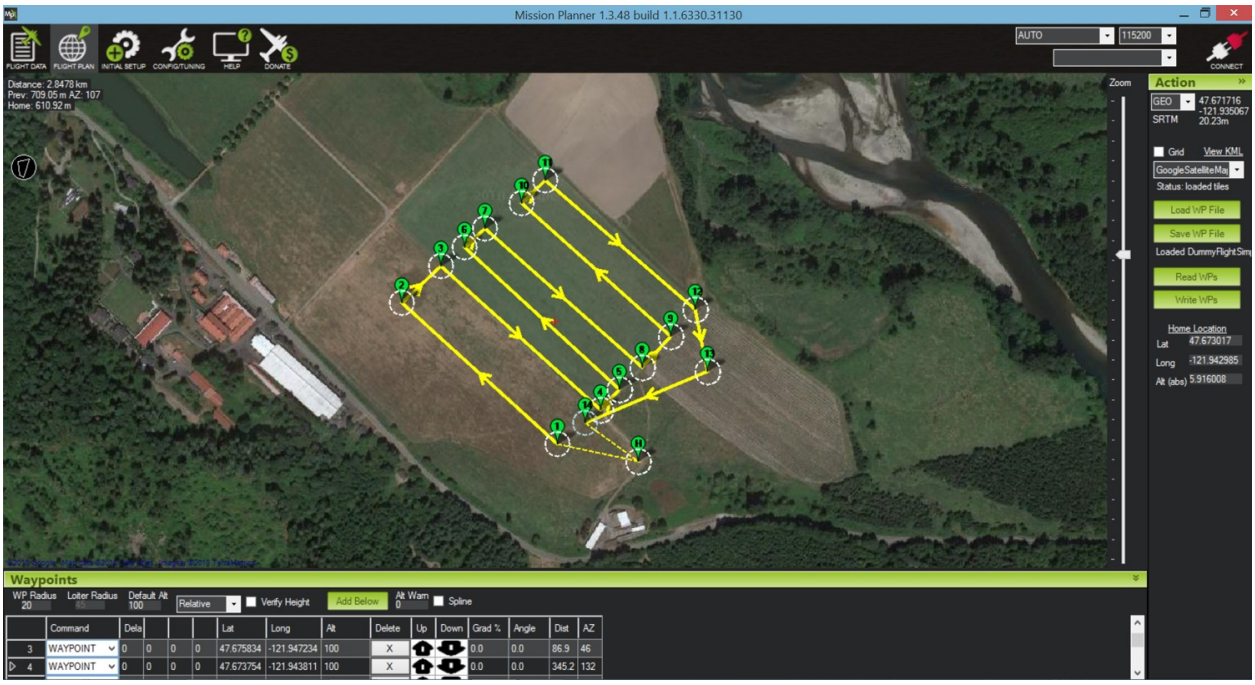

Fig. 11: A sample waypoint file used for flight control in Mission Planner software.

Mission planner was also used to auto-land the aircraft to minimize the already heightened risks of flight testing in the middle of the night. Data logged during flight was used during post-processing of data to determine the location of the aircraft at different times in order match the location of the aircraft with the attached time stamps on images, thus enabling the determination of which images were taken where on the flight path. This in turn showed what test article corresponded to each image.

5. Custom Payload

The camera and lens chosen for the payload were a Blackfly 2.0 MP Mono GigE PoE camera and ThorLabs MVL35M1 fixed 35 mm lens. These were selected based on mass requirements, power consumption, resolution, and budget. Fixed mounts were 3D printed and used to attach the camera to the nose of the aircraft. The camera was connected to the Rasperry Pi running an Ubuntu Mate OS via an Ethernet cable, and the camera interface was managed using the software FlyCapture 2, provided by Blackfly. In order to run the collection scripts, manage images, and troubleshoot while the Raspberry Pi was inaccessible inside the UAV, the Raspberry Pi was set up to broadcast an ad hoc network. This allowed remote desktop access to the Raspberry Pi desktop with a laptop, which we used to initiate scripts at the start of all tests. The image acquisition script was written in C++, and allowed configuration of several variables including the desired number of images, delay between images, and the shutter speed of the camera. The mass of the final payload including power sources was roughly 400 grams.

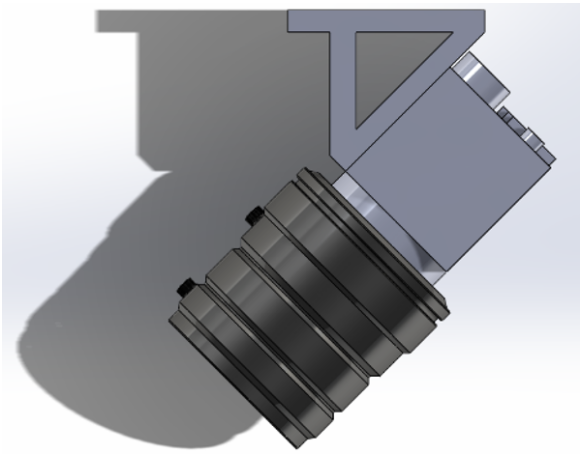

Fig. 12: A 3D model of the camera and lens on a fixed mount.

B. Experimental Methods

Once the design of the payload was completed, it was necessary to begin testing the payload. In order to accomplish this, three different types of testing were completed. First, feasibility testing was completed with a Canon Rebel T5i, to ensure that the concept was viable before further development work or purchases were made. Once this was finished, further developments were made to the design of the payload and the camera, lens and other necessary equipment was procured. After the equipment was assembled, the group began a series of ground tests to further explore feasibility and gauge expected results for the final series of tests, the flight testing. Flight testing was the critical stage of testing, as this was the stage that would determine the viability of the payload while in use for its true application. In each phase of testing, a variety of performance metrics were used to evaluate performance and feasibility.

1. Performance Metrics

The assessment of payload performance followed two main avenues: human operator assessment and Signal to Noise Ratio (SNR). Original criteria from the project sponsors required that a human should be able to compare data from a field with a poacher and a field without a poacher and decisively recognize a difference. In order to further quantify the data, signal to noise ratio was used to analyze the detectability of light in images. A minimum SNR for detectability was set to be 5, with a signal size of at least 0.05% of total pixels. The higher the signal to noise ratio is, the more detectable the signal will be. Signal to noise ratio and signal size are impacted by mounting angle of the camera, flight altitude, and camera parameters. By monitoring changes in the SNR across various tests, it was possible to evaluate the impact of these variable parameters on payload performance. Study of these relationships enabled recommendations for how the payload should be implemented to maximize performance.

Simulated images of data for SNR and signal size above, below, and near the performance threshold are shown in Fig. 13. For varying SNR the signal size is kept constant at 0.5%, while for varying signal size the SNR is kept constant at 5. Blur is also introduced to simulated data to better represent how actual results may appear.

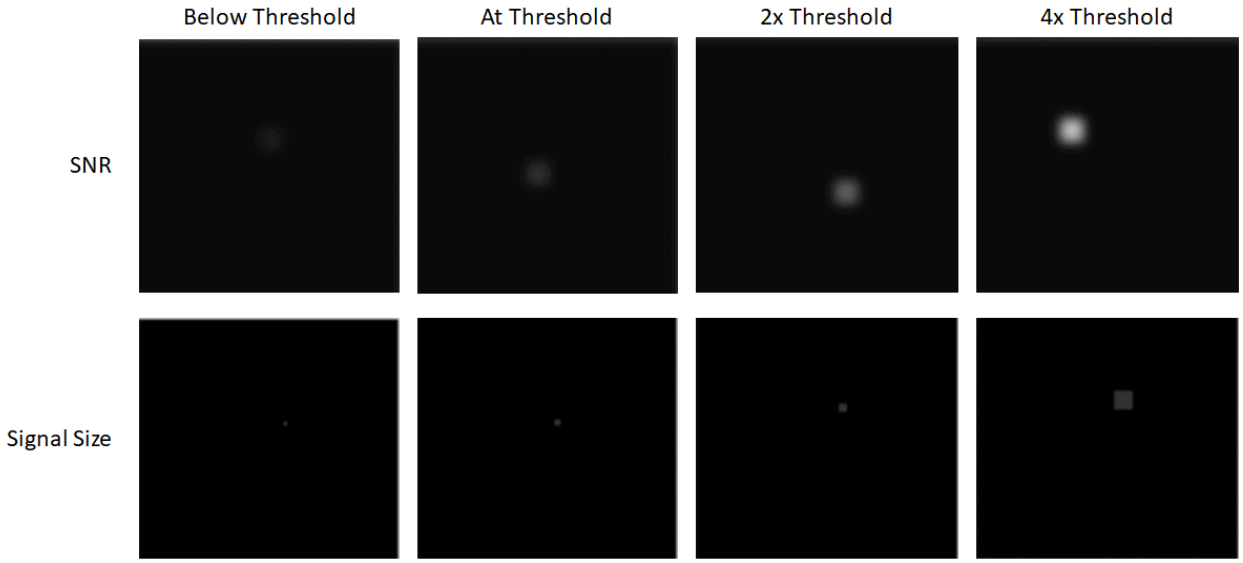

Fig. 13: Simulated data near, above, and below the performance threshold for SNR and signal size.

2. *Ground Testing*

Ground tests were conducted in order to compare initial results to theoretically predicted values, establish an initial idea surrounding the feasibility of the payload, to flush out issues with the payload and to give an expectation of results for flight testing. Ground tests were conducted by reflecting different types of flashlights off of a surface that was perpendicular to the ground. Blankets were used in order to establish a better surface for light reflection, however the albedo of these blankets were higher than the expected albedo of grassland or savanna, but this heightened albedo was accounted for as will be discussed in the results section. Different light sources were used to illuminate the perpendicular surface and then images were taken of the light sources from varying distances ranging from 80 meters to 180 meters. Ground tests were also conducted on different nights to take advantage of different ambient lighting conditions, but due to the proximity of the ground test site to the city of Seattle, light pollution minimized the impact of differing ambient light conditions. This will be discussed in more detail in the results section. Camera settings were also varied during ground tests.

3. *Flight Testing*

Flight testing was the final phase of testing that was completed. Flight tests were conducted in order to gather data about the payload performance in an environment that simulated the environment it is meant to be deployed. Flight tests were completed at UW Carnation UAS Test Site (UWCUTS) in Carnation, Washington. This area was a large grassy field with plenty of space for flying the aircraft. Due to the necessity of flying at night, flight tests were conducted under FAA Certificate of Waiver 1070W-2018-10815 which waived 14 CFR §107.29. In addition, before conducting flight tests, risk assessments[16] were performed to ensure safe operations[17] at night were feasible.[18]

Initially, aircraft stability was tested with a dummy payload to ensure stable flight could be achieved with the artificial light detection payload. These dummy flights were successful so testing proceeded with the real payload. Tests were completed on four separate days. Flights with the final payload were made during daylight initially to verify its functionality in the air, and then the team began conducting feasibility testing.

The parameters varied for flight tests were ambient conditions, the test article, the angle the camera was mounted, the altitude of the flight path and the shutter speed of the camera. Varied ambient conditions and test articles allowed the team to test performance under different scenarios, helping establish a more complete understanding of payload performance. Altering the angle the camera was mounted was done in order to find a balance between seeing the largest area on the ground possible and ensuring that area was not too large such that lights would not be seen clearly. Increasing the size of the viewed ground area increases

the chance of detecting a light, so it was necessary to attempt to establish an optimum viewing angle to maximize viewed ground area and keep the probability of detection high.

C. Results

1. Ground Testing

Ground tests were completed with sensor mounted on a tripod facing toward a reflective surface (with an approximate albedo of 0.4). The surface remained fixed and the camera was moved away from it to distances ranging from 80 m to 180 m. Tests were also completed on a cloudy night and a clear night, and with two different camera apertures.

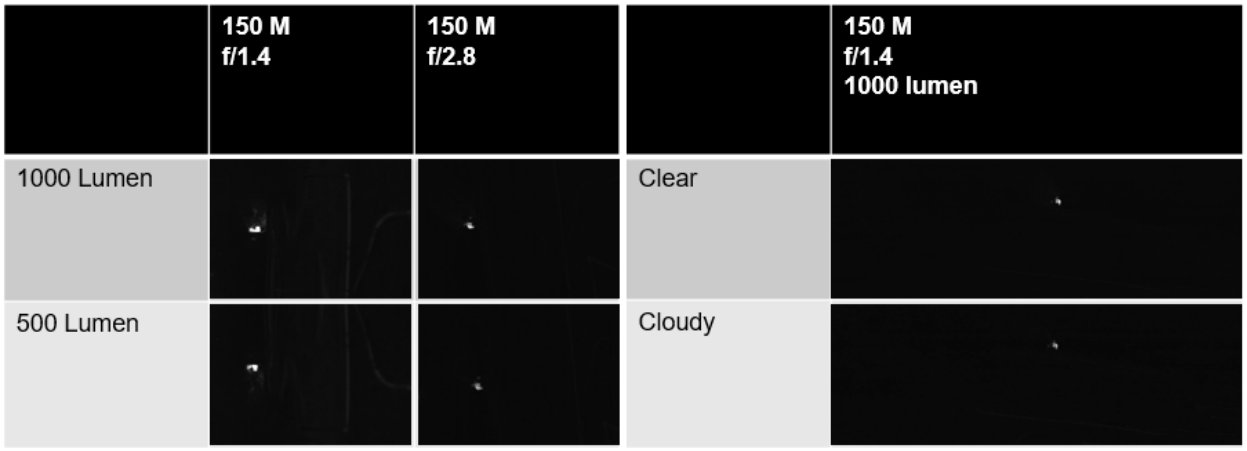

Fig. 14: A sample of results obtained while testing the sensor package on the ground.

Two different flashlights were used for testing, a 500 lumen and a 1000 lumen, both with beam widths of approximately 50 degrees. Samples of test results are shown in Fig. 14. The reflective surface used for ground testing was significantly smaller than the background behind it, leading to an oddly shaped light in the data sets. This negatively impacts the visibility of the reflected light as distance is increased, as the amount of pixels corresponding to the lit reflective surface is much smaller than the amount of pixels corresponding to a flashlight shone towards the ground.

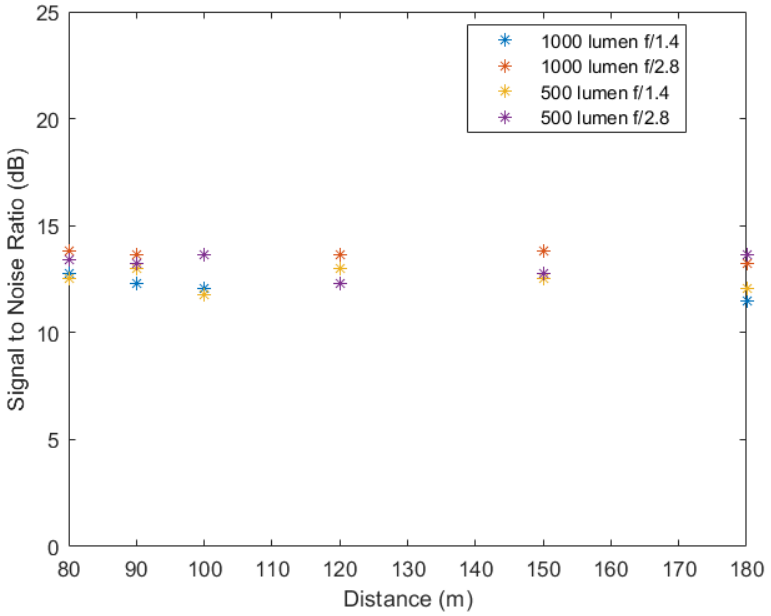

Fig. 15: Signal to noise ratios found at varying distances, flashlight brightness, and camera aperture.

The SNR was found to be slightly less than 10% of the original predicted value of 151, as a saturation cap was not originally taken into account during computations. In all data sets, the peak value was fully saturated on the camera (a maximum value of 255). To address this, a saturation cap was introduced to feasibility calculations, resulting in a new prediction of a SNR of approximately 10. The signal to noise ratio found for each light source at varying exposures and distances is shown in Fig. 15. As expected, signal to noise ratio was not found to vary significantly with distance, only the size of the reflected area (which does not impact the signal to noise ratio).

Table 2: Average signal to noise ratio of each test.

	SNR
500 lumen at f/1.4	12.38
500 lumen at f/2.8	13.62
1000 lumen at f/1.4	12.51
1000 lumen at f/2.8	13.17
Predicted, with saturation cap	12.04

The average SNR for each trial is also shown in Table 2. The difference between the predicted SNR and the recorded SNR may be due to differences caused by a small, more reflective patch as opposed to a reflection on a flat surface that is less reflective. Additionally, the theoretical computations are designed assuming the the ground is relatively similar in albedo, not for a more reflective bright area. The average is taken across all the distance trials, where the signal to noise ratio is found not to vary significantly. The flashlight brightness does not appear to consistently change the signal to noise ratio, as with a fully saturated peak, the two appear equally bright in pictures. This is also why there is a more significant different between the two at the narrower aperture. Comparatively, narrowing the aperture does increase the signal to noise ratio by 5 to 10 percent.

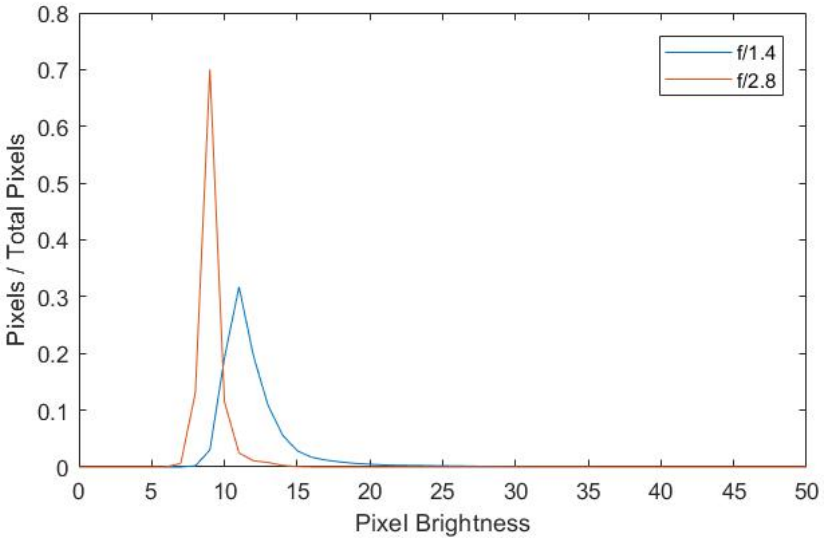

Fig. 16: Noise magnitude and occurrence frequency compared between apertures; samples from 150 m test with 500 lumen light source.

As shown in Fig. 16, the SNR is lower for wider apertures, because the larger aperture lets in more light from the signal (which is already fully saturated), and more light from the noise (which increases the average noise value, and thus, the SNR). This concept is discussed in section II, subsection C. Using an aperture of f/1.4 was found to produce less noise but of a higher magnitude, while an aperture of f/2.8 produces more noise of a lower magnitude. To increase overall probability of detection, the SNR should be as high as possible, which requires keeping the noise as low as possible while keeping the signal fully saturated. Fine tuning the exposure value while ground testing is difficult due to external factors like viewing the sky itself, and testing near large amounts of light pollution, which increase the background noise. As such, further attention was devoted to this during flight testing.

Shutter speed for the ground tests was taken at 1/100, though this will be decreased to 1/300 as a starting point for flight testing. This change in shutter speed is projected to increase the SNR of resulting data by fifteen percent.

Higher sky luminosity in Seattle (versus Botswana) is predicted to increase the SNR of results in Botswana by 0.5%. A cloudy night is predicted to have a 10% higher SNR than a clear night, but due to reflected light off of clouds, only a 0.3% difference was observed. Adjusting for albedo in Botswana versus albedo of material used for ground test reflection decreases the SNR by 5%. Comparing the theoretical case in Botswana, with a SNR of 14.5, to the average SNR from ground testing signal of approximately 12.9, the signal to noise ratio in Botswana is expected to be approximately 12% higher than ground testing results.

2. Flight Testing

Flight tests were completed by mounting the sensor on a fixed angle mount inside the nose of a UAV and flying a circuit over several known light sources. Before any night tests were conducted, several day tests were completed to ensure functionality of all systems. During a day test, images were captured to demonstrate the resolution of the camera. These images are shown in Figure 17. The SUV can be clearly identified in the left image, but correctly identifying people is much more difficult. Thus, the camera is not recommended for day time object classification due to lack of sufficient resolution.

The flight path for all testing is shown in Figure 18, along with samples of where images with light in them were taken for one test. A 500 lumen flashlight was placed near waypoint 4 (denoted by a green marker with a 4 on it), a 1000 lumen flashlight near waypoint 8, and car headlights near waypoint 12. In Figure 18 blue numbered circles denote images taken with light on them; so images one and two are of the 500 lumen light source, image three is of the car headlights, four and five are of the 1000 lumen light source, and six through nine are of the car headlights. A matrix of all tests completed is shown in Table 3.

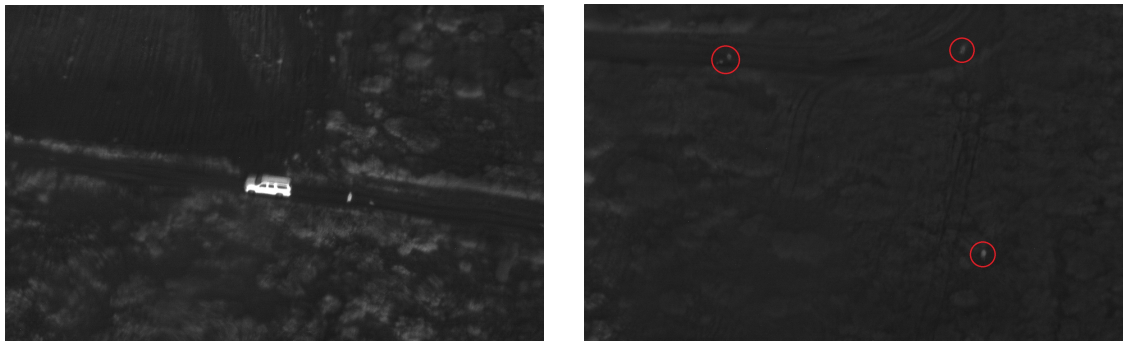

(a) A SUV imaged with a person standing next to it.

(b) Three people imaged, two on a road and one in the field.

Fig. 17: Daylight images taken to demonstrate camera resolution.

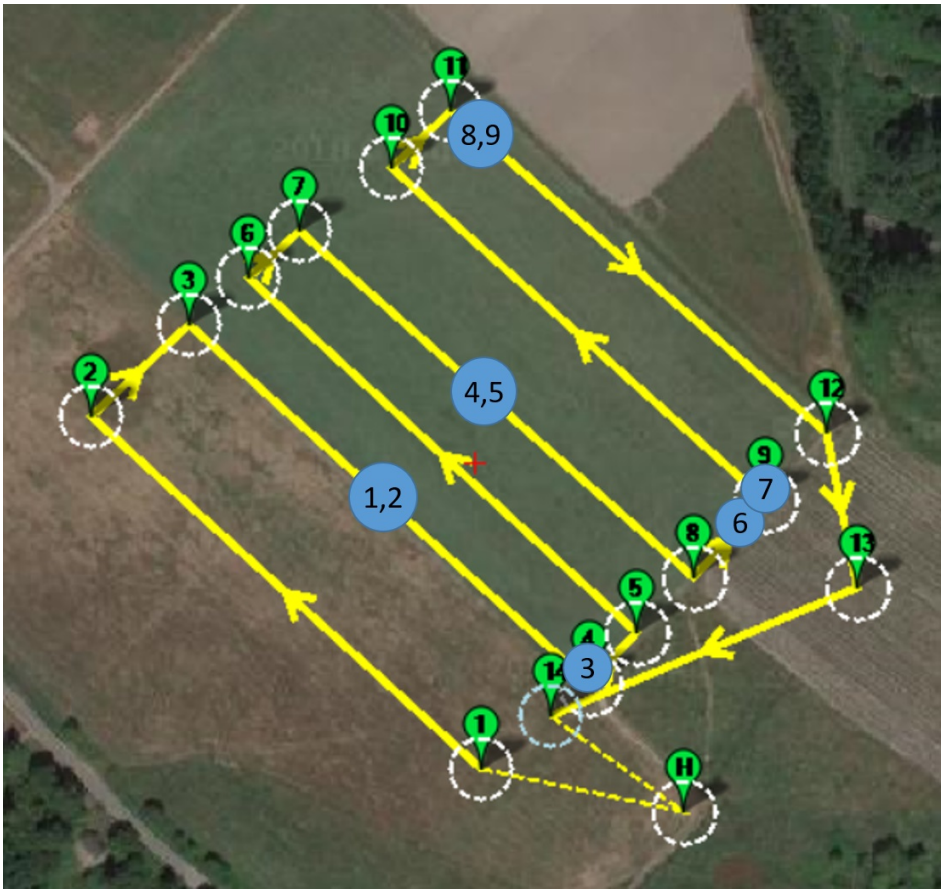

Fig. 18: A sample of the locations of images with light in them (indicated by number in blue circles), taken during night test three.

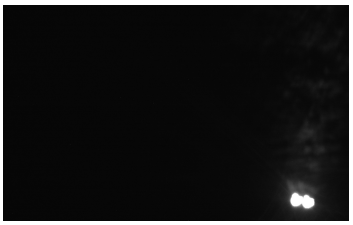

(a) Car headlight seen directly and reflected.

(b) Flashlight reflected on ground.

(c) Flashlight seen directed at camera.

(d) Flashlight reflected on ground, seen with long shutter speed.

(e) Two flashlight seen reflected on the ground, 500 lumen and 1000 lumen brightness seen from left to right; Test 7 image.

(f) Test image with no light imaged.

Fig. 19: Sampling of night testing images.

Table 3: Flight testing matrix.

	Shutter Speed	Mount Angle	Weather	Notes
Test 1	1/333 s	60 deg	cloudy	
Test 2	1/50 s	60 deg	cloudy	
Test 3	1/12.5 s	60 deg	cloudy	
Test 4	1/10 s	60 deg	cloudy	no car headlights
Test 5	1/5 s	60 deg	cloudy	no car headlights
Test 6	1/333 s	45 deg	clear	
Test 7	1/50 s	30 deg	clear	
Test 8	1/50 s	45 deg	clear	
Test 9	1/50 s	60 deg	clear	
Test 10	1/667 s	60 deg	clear	
Test 11	1/50 s	60 deg	foggy	
Test 12	1/5 s	60 deg	cloudy	flashlight directed at camera

Samples of images taken while flight testing are shown in Figure 19. In test images, car headlights are consistently the easiest to identify. The reason for this is twofold: two lights next to each other are easy to differentiate from a single light source, and because the lights are designed to illuminate as much road as possible, they are angled almost parallel to the ground, casting a long strip of light across the field. Comparing images a and b, it is clear that the car is casting a much larger beam than the flashlight, which appears as a small triangle.

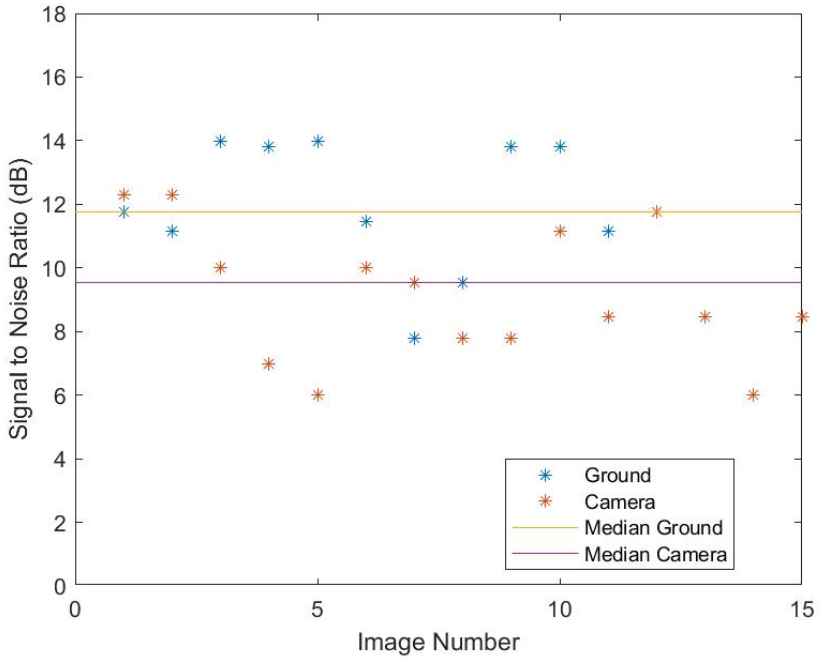

Fig. 20: Plot demonstrating variation of signal to noise ratio with light directed at camera versus at the ground.

Lights pointed directly at the camera were also consistently easy to identify, though that is not expected to be a general operating condition. However, images with the flashlight directed at the camera have a slightly lower signal to noise ratio than images with flashlights directed at the ground. This is due to the increase in background noise caused by scattering photons from the flashlight directed at the camera that serve to increase the background noise and make the image brighter on the whole. A plot of the signal to noise ratio compared between the two cases is shown in Figure 20. The average signal to noise ratio for the case with flashlight pointed at ground is almost 2 dB higher than the that of the case with the flashlight pointed at the camera. However, much more variation in the SNR is found in images with the flashlight pointed at the camera. The theoretical SNR for both cases was predicted to be 11.88 dB, as the signal is expected to be fully saturated for both, and the noise is expected to be constant, as only environmental and camera factors are considered in theoretical noise computations. The median SNR for the case where the lights were aimed at the ground was recorded as 11.76 dB, a 1% discrepancy, and for the case where the lights were aimed at the camera the median SNR was recorded as 9.54 dB, a 20% discrepancy. The difference for the light pointed at the ground case is likely due to environmental factors (slightly darker or brighter than predicted). The much larger difference for the light at the camera case is likely due to the increased noise discussed above, as well as operator error in keeping the flashlight pointed directly at the camera, leading to some images with it slightly skewed.

Increasing the shutter speed significantly to cause blurred images was also investigated as a detection method, shown in Figure 19d, where the light source is seen blurred across the upper right corner. These images also tended to have a lower signal to noise ratio due to higher background noise induced by the long shutter speed. A plot of the signal to noise ratio compared between shutter speeds is shown in Figure 21. The data is presented in a semi-log scale, because the shutter speeds tested were not linearly spaced. Two data fits are shown; the first fits shutter speeds between 3 and 200 ms, and the second fits the origin and the two lowest shutter speeds. This is done to demonstrate the sharp increase of SNR with shutter speed as the light first becomes visible in the images (at incredibly low shutter speeds, no light is let in to the camera sensor, so the image appears entirely black), as well as the slower decrease in SNR as the shutter speed increases once the peak signal is already fully saturated. The intersection between these two fits suggests that the SNR stops increasing with shutter speed at approximately 1/333 seconds, or 3 ms. All of the images for night testing were taken at an aperture of f/1.4, so this suggests that an optimal EV for detection is

approximately 9.35.

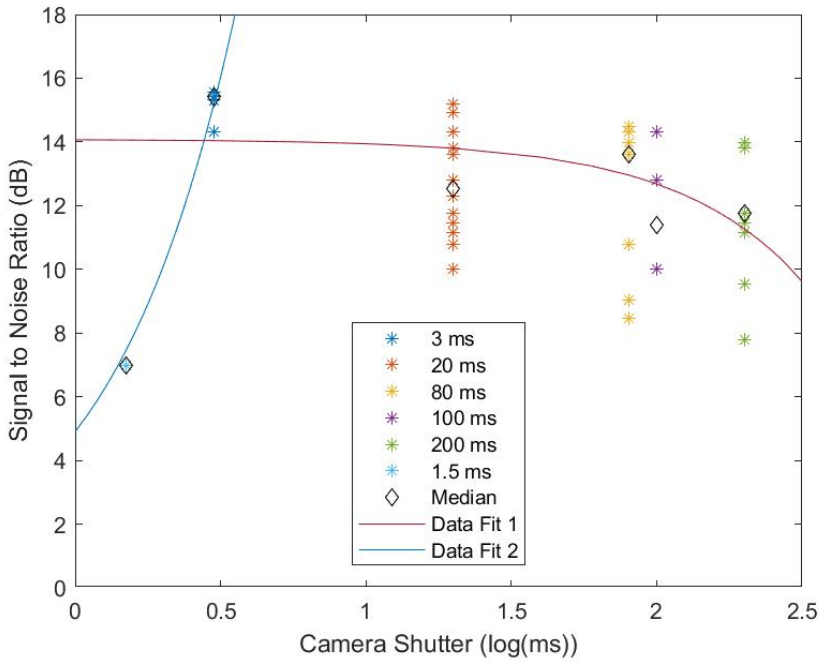

Fig. 21: Plot demonstrating variation of signal to noise ratio with shutter speed.

A comparison of theoretical SNR to recorded SNR for shutter speed trials can be found in Table 4. The theoretical predictions perform well for the most part, but quickly lose accuracy as the shutter speed is decreased past the point where the camera is no longer fully saturated by the signal. This indicates that the camera may not be performing entirely to its provided specifications, or incorrect estimations of reflected wavelength. For computations, the wavelength was assumed to be constant based on the output of the flashlight, but in reality wavelength is impacted by the medium that the light is reflected off of. Outside of the high error for the two low shutter speed values, the theoretical roughly matches the recorded. For most higher shutter speeds, a relatively large spread of data is obtained, with the theoretical well inside of it.

Table 4: Camera shutter SNR theoretical comparison to recorded.

Shutter Speed	Theoretical SNR (dB)	Recorded SNR (dB)	Discrepancy (%)
1/667 s	12.03	6.99	41.9
1/333 s	12.03	15.44	-28.3
1/50 s	12.01	12.55	-4.5
1/12.5 s	11.97	13.62	-13.8
1/10 s	11.95	11.39	4.7
1/5 s	11.88	11.76	1.0

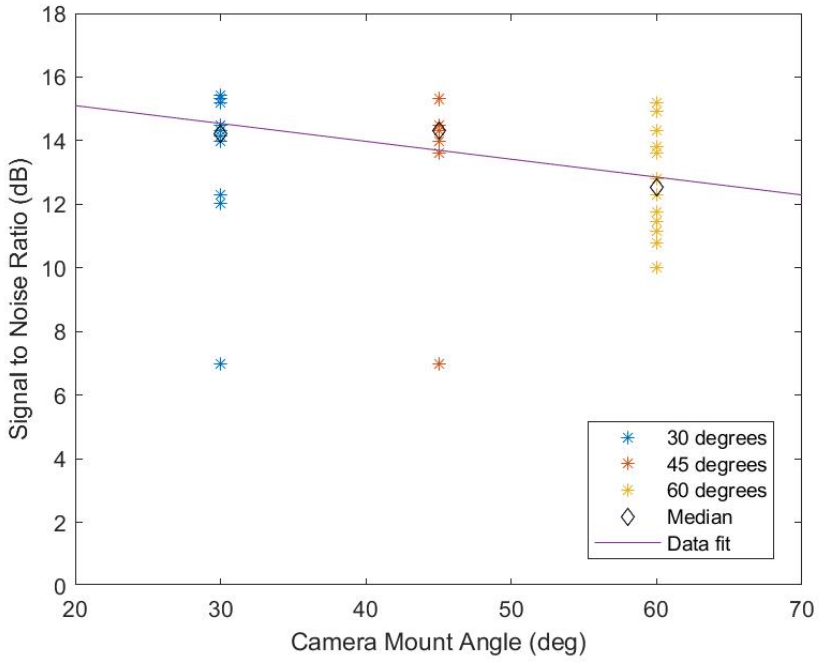

Fig. 22: Plot demonstrating variation of signal to noise ratio with camera mount angle.

Multiple camera mount angles were also tested to attempt to cover the largest ground area possible. The mount angles (measured from the horizontal) tested were 30, 45, and 60 degrees. A plot of the resultant signal to noise ratios is shown in Figure 22. The SNR was found to decrease approximately linearly with angle, but the amount of images captured with light in them decreased similarly. That is to say, with smaller mount angles, more ground is visible so the light appears smaller relative to it and is detected less often, but has a higher signal to noise ratio when it is detected, while larger angles are more likely to detect dimmer lights. The size of the camera footprint for each mount angle is shown in Table 5. Theoretical computations did not take into account camera mount angle, so these results cannot be compared to expected values; however, the results are in line with the SNR obtained from other trials.

Table 5: Ground footprint of area captured for each camera mount angle (measured from the horizon) at operating altitude of 120 m.

	Image Width	Image Height	Image Area
60 deg	38.58 m	32.25 m	1244.21 m^2
45 deg	38.58 m	48.71 m	1879.23 m^2
30 deg	38.58 m	99.45 m	3836.78 m^2

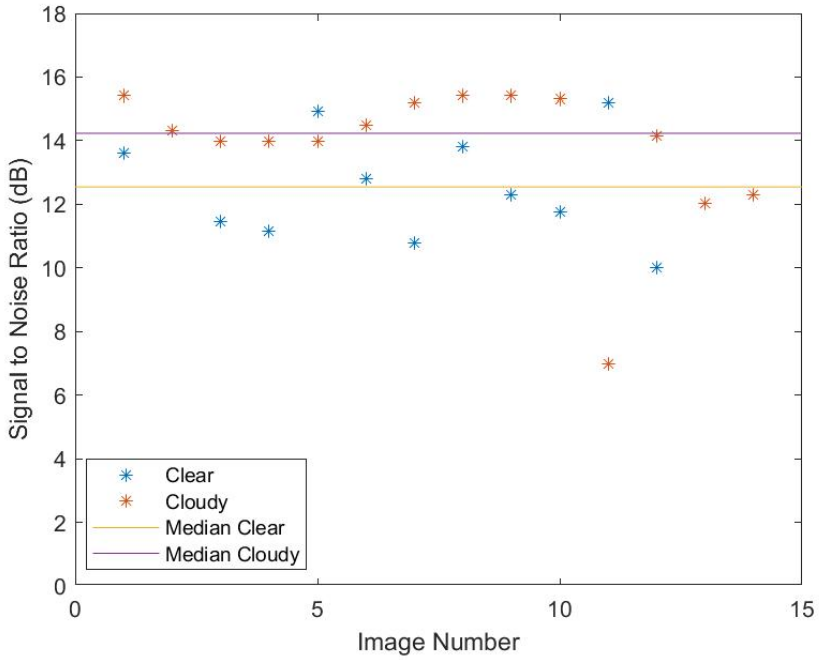

Fig. 23: Plot demonstrating variation of signal to noise ratio with clear and cloudy weather conditions.

The impact of weather on signal to noise ratio was also tested, and results are shown in Figure 23. The median signal to noise ratio was found to be significantly higher for cloudy nights than for clear nights, which is the opposite of results from ground testing, but the expected result nonetheless. The ground tests were conducted much closer to large sources of light pollution, so there was much more ambient light reflecting off of the bottom of the clouds in those cases. This would have lowered the SNR for cloudy cases compared to the flight tests, where there was less ambient light to reflect off the bottom of the clouds, increasing the signal to noise ratio. The predicted difference between clear and cloudy conditions was 2.0 dB; with a recorded difference of 1.68, the 15% discrepancy is likely due to the presence of more light pollution in Washington than in Botswana.

3. Image Classification and Probability of Detection

Probability of successful poacher detection is comprised of three separate components: getting an image with a poacher in it, detecting the poacher in the image, and successfully classifying the image as one with a poacher in it. Detecting the poacher is governed by SNR and signal noise, and has been discussed in the previous section. Assuming that the sensor is operated at the ideal parameters derived in the previous section, the signal to noise ratio is not a limiting factor in detection. Getting an image with a poacher in it is governed mainly by the camera mount angle and the chosen flight path of the UAS. Because the flight path and duration of the final payload is outside of the scope of this project, that component is neglected in further analysis.

Successful classification of the image is dependent on an algorithm recognizing the light source within it as something other than background noise. This classification was completed by finding the median pixel brightness in an image, and searching for pixels a given amount brighter than the median brightness that are grouped together. As the distribution of background noise in an image nominally follows a bell curve type distribution, as shown in Figure 16, searching for values 2.5 median standard deviations above the median returned all images with light sources in them for all test cases.

Directing the light at the camera did introduce some additional background noise to images that did not have the light source directly imaged. Light from the flashlight, while not captured in a solid beam in the camera, appeared to reflect off of the nose cone or internal camera mechanisms and caused a beam reflecting across the middle of the image. This type of distortion could also be caused by any light sources reflecting off of water or highly reflective surfaces outside of the area being imaged. For this reason, these images are

considered to be false flags, and account for 3% of total images with light detected. An example of a false positive is shown in Fig. 24, along with a positive and negative classification.

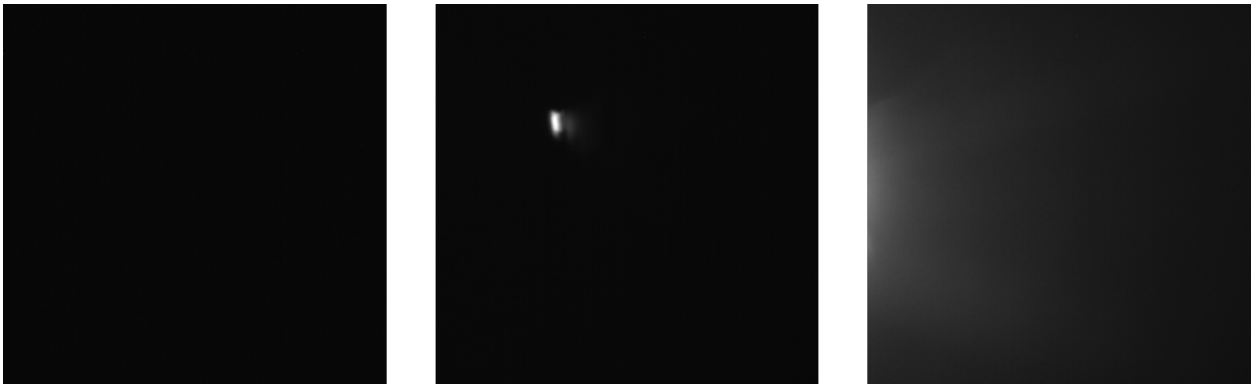

Fig. 24: Sample images of a negative, positive, and a false positive classification, shown from left to right.

The odds of an image having a poacher determined by the ground area covered by the camera at a given mount angle. The total probability of detection also relies on the amount of images captured by the camera (corresponding to the same fixed light sources), and these two metrics are used to compare the different mount angles. The 45 degree and 30 degree mounts far outperformed the 60 degree mount by these metrics, though the performance of the 45 and 30 degree mounts are similar. This indicates that the ideal mount angle may be somewhere between these angles.

The probability of detection is simply the multiple of the probability of the three conditions required for detection. The probability of getting an image with a poacher in it is simplified as the fraction of ground area covered in an image to the the total ground imageable by the sensor package on the flight path. In experimentation, all images were found to overlap at least 30% with the previous image, regardless of camera mount angle, so the probability of the ground being imaged is 100%. The probability of successful classification is defined as the probability of light detection minus the probability of false flags, or 97%. As mentioned above, the SNR and signal size were found to be well above detection thresholds for all cases, to the probability of successful detection of the poacher is taken to be 100%. This yields a total probability of detection of 97 %.

IV. Conclusion

A light detection sensor payload was successfully developed and tested while meeting customer specifications. The total mass of the payload was approximately 400g, well bellow the maximum 1 kg requirement. The payload was also easily integrated into a Fixed Wing Sabre plane, and would be presumably simple to integrate into one of Vulcan Inc.'s unique aircraft. Finally the project cost approximately 3000 dollars, which was substantially bellow the total budget. When flight tested, the sensor was convincingly able to identify both the 500 and 1000 lumen flashlights as well as car headlights at 120m AGL under various conditions.

Data analysis produced several distinct observations based on the tested variables. The system successfully functioned under clear and cloudy skies, though the SNR was higher during cloudy conditions. It was also found that as the camera mount angle increased SNR slightly decreased while probability of detection increased. Additionally, light sources pointed at the ground had a higher probability of being detected than those pointed directly at the UAS. SNR also increased with shutter speed until the sensor was fully saturated, where it then began to decrease with increasing shutter speed. The optimal EV for detection was also determined to be approximately 9.5.

With the success of this proof-of-concept, there a re a few next steps to take in order to finalize the prototype. The first step consist of further optimizing and streamlining the system. Vulcan Inc. has indicated that they will work to allow all image processing to be done on-board while the UAS is in flight, and to be able to send real time pings to rangers when poachers are detected. This would also require the development of a long range network connection so that the UAS could send notifications and data if needed. These are all expected to be included in Vulcan Inc.'s upcoming V2 UAS, where this payload could

be integrated.

Since the Pacific Northwest is not entirely representative of the intended operating conditions, additional flight tests should be conducted in Botswana in order to ensure the system performs exactly as intended. The most notable changing condition is light pollution, as the African savanna will have considerably less artificial light than the greater Seattle area. Additionally, it is worth considering that the change in ground material may affect albedo values and cause slight SNR variation.

V. Acknowledgements

Our team would like to graciously thank the Vulcan development team for their support and guidance in this project.

We would also like to thank and acknowledge contributors from the UW including various researchers at the AFSL, Hannah Rotta, Professor Kristi Morgansen, and the entire UW AA department for their continuing support in this project. We would also like to thank Jill Dalinkus for interacting with our industry sponsors and supporting the program.

Finally, we would like to thank Carnation Farms for supporting this and many other educational and research projects at their facility.

References

[1]Orenstein, R., *Ivory, Horn and Blood: Behind the Elephant and Rhinoceros Poaching Crisis*, Firefly Books, 2013.

[2]Scriber, B., "100,000 Elephants Killed by Poachers in Just Three Years," *National Geographic*, Vol. 18, 2014.

[3]Mulero-Pázmány, M., Stolper, R., Van Essen, L., Negro, J. J., and Sassen, T., "Remotely piloted aircraft systems as a rhinoceros anti-poaching tool in Africa," *PloS one*, Vol. 9, No. 1, 2014, pp. e83873.

[4]"Air Shepard," `http://airshepherd.org/`, Accessed June 6, 2018.

[5]Nuwer, R., "High Above, Drones Keep Watchful Eyes on Wildlife in Africa," *New York Times*, March 2017.

[6]Lum, C. W., Vagners, J., and Rysdyk, R. T., "Search Algorithm for Teams of Heterogeneous Agents with Coverage Guarantees," *AIAA Journal of Aerospace Computing, Information, and Communication*, Vol. 7, January 2010, pp. 1–31.

[7]Lum, C. W. and Vagners, J., "A Modular Algorithm for Exhaustive Map Searching Using Occupancy Based Maps," *Proceedings of the 2009 Infotech@Aerospace Conference*, Seattle, WA, April 2009.

[8]Nigam, N., Bieniawski, S., Kroo, I., and Vian, J., "Control of Multiple UAVs for Persistent Surveillance: Algorithm Description and Hardware Demonstration," *Proceedings of the AIAA Infotech@Aerospace Conference*, Seattle, WA, 2009.

[9]Lum, C. W., Summers, A., Carpenter, B., Rodriguez, A., and Dunbabin, M., "Automatic Wildfire Detection and Simulation Using Optical Information from Unmanned Aerial Systems," *Proceedings of the 2015 SAE Aerotec Conference*, Seattle, WA, September 2015.

[10]Lum, C. W., Mackenzie, M., Shaw-Feather, C., Luker, E., and Dunbabin, M., "Multispectral Imaging and Elevation Mapping from an Unmanned Aerial System for Precision Agriculture Applications," *Proceedings of the 13th International Conference on Precision Agriculture*, St. Louis, MO, August 2016.

[11]Xu, S., Kraus, C., and Lum, C. W., "Generating Multi-Purpose Rendered Environments from Unmanned Aerial System Data," *Proceedings to the AIAA Information Systems-AIAA Infotech@ Aerospace*, Kissimmee, FL, January 2018.

[12]"Wildeas," `https://www.wildeas.org/about`, Accessed June 6, 2018.

[13]Worland, J., "Drones Are Helping Catch Poachers Operating Under Cover of Darkness," *Time*, Vol. 31, May 2018.

[14]Fei Fang, e. a., "Deploying PAWS to Combat Poaching: Game-theoretic Patrolling in Areas with Complex Terrain," January 2016.

[15]L, W., "51.85 Billion Unmanned Aerial Vehicle (UAV) Market to 2025," *Buisness Wire*, May 2018.

[16]Lum, C. W. and Tsukada, D. A., "UAS Reliability and Risk Analysis," *Encyclopedia of Aerospace Engineering*, July 2016.

[17]Lum, C. W. and Waggoner, B., "A Risk Based Paradigm and Model for Unmanned Aerial Vehicles in the National Airspace," *Proceedings of the 2011 Infotech@Aerospace Conference*, St. Louis, MO, March 2011.

[18]Lum, C. W., Gauksheim, K., Kosel, T., and McGeer, T., "Assessing and Estimating Risk of Operating Unmanned Aerial Systems in Populated Areas," *Proceedings of the 2011 AIAA Aviation Technology, Integration, and Operations Conference*, Virginia Beach, VA, September 2011.